Steady and Unsteady Transonic Pressure Distributions on NACA 0012

Hermann Triebstein*
Deutsche Forschungs-und Versuchsanstalt für Luft und Raumfahrt e.V., Göttingen, FRG
Institut für Aeroelastik, Göttingen, West Germany

Steady and unsteady aerodynamic data were measured on a two-dimensional model with an airfoil of 12% thickness mounted in the transonic wind tunnel of the DFVLR in Göttingen. The profile was oscillated in pitch about its c/4 axis to generate the unsteady aerodynamic pressure data. The primary purpose of the wind tunnel test was to measure data for use in the development and assessment of transonic analytical codes and to show the dependence of aerodynamic responses on the following parameters: Mach number (0.5-1.0), reduced frequency (0.2-0.12), angle of attack (0-9 deg), and oscillation amplitude (0.5-2.5 deg). Emphasis is also placed on the nonlinearities that actually occur and that are peculiar to higher angles of attack. Steady and unsteady calculation results agreed fairly well with the measured data.

Nomenclature

a = sonic speed
c = wing chord
c_p = nondimensional pressure coefficient [$= (\bar{p}-p_0/q]$
c_{p_b} = amplitude function of pressure coefficient for pitching oscillations
c'_{p_b}, c''_{p_b} = real and imaginary parts of the nondimensional and standardized pressure coefficient for pitching oscillations [$= p/(q \cdot \Delta\alpha)$]
c_p^* = critical pressure coefficient
Δc_p = unsteady load distribution
f = oscillation frequency
M = freestream Mach number ($= V/a$)
$\bar{p}$ = steady pressure
p = unsteady pressure
p_0 = stagnation presure
q = dynamic pressure ($= \rho V^2/2$)
Re = Reynolds number ($= Vc\rho/\mu$)
V = steady freestream velocity
x,y,z = Cartesian coordinates, see Fig. 1
α = angle of attack
$\Delta\alpha$ = pitching oscillation amplitude in radian measure
ρ = air density
μ = dynamic air viscosity
ω = angular frequency ($= 2\pi f$)
ω^* = reduced frequency ($= \omega c/2V$)

Introduction

IN addition to information on the elastic behavior of a structure, it is necessary that the unsteady aerodynamic forces acting on the structure are known in order to guarantee the aeroelastic stability of any kind of aircraft. Knowledge of these unsteady aerodynamic forces requires in turn an understanding of the steady forces. At the present stage of aircraft development, it is imperative that particular attention be drawn to the realm of transonic flow and the separation phenomena that occur therein. Special interest is focused on supercritical wings and control surfaces of active control systems.

Received March 25, 1985; revision received Nov. 6, 1985.

*Senior Research Engineer, Institute of Aeroelasticity.

In the theoretical sector, modern computers have facilitated gradual access to the transonic flow range. Correspondingly, this paper is devoted to experimental determination of the steady and unsteady pressure distributions on a NACA 0012 profile in order to develop ideas on how to improve present theoretical approaches and calculation methods. The NACA 0012 profile was chosen for this investigation because it appears on the list of the Working Group of the AGARD Structures and Materials Panel and because results of other investigations on this profile are available for comparison purposes.[1] In this paper, several sources dealing with measurements on the NACA 0012 profile are presented.

Above all, the measured data are meant to demonstrate the dependence of the aerodynamic responses on known parameters. Moreover, the nonlinearities that actually occur are clearly shown because in most of the known experiments no attempt has been made to measure any of the higher harmonics although large nonlinearities have been known to occur at a shock wave. Most of the sources dealing with these problems are given in Ref. 2. The measurements were performed in March 1982 in the transonic wind tunnel of the DFVLR in Göttingen, West Germany.

Wind Tunnel

The transonic wind tunnel of the DFVLR in Göttingen is a closed-circuit, continuous-flow tunnel, which has a 1-m × 1-m test section with perforated walls. Mach number and the dynamic pressure, and thus the Reynolds number, can be varied simultaneously or independently, with air as the test medium.

Test Setup and Wing Configuration

A schematic diagram of the test setup is shown in Fig. 1. The test model is supported on either side by ball bearings outside the perforated wind tunnel walls. Excitation of the model to perform pitch oscillations about its c/4 axis is achieved by means of a hydraulic rotation cylinder, the pump of which is located outside the wind tunnel. A coupling mechanism provides a rigid connection in the radial direction while relieving the hydraulic cylinder in the axial direction. An angle-of-rotation pickup is mounted outside the wind tunnel wall, allowing the angle of attack as well as the pitch oscillation amplitude to be adjusted and monitored.

The wing instrumentation consists of 30 differential pressure transducers (Kulites, ±5 psi), 4 accelerometers, and 2 angle-of-rotation pickups. The transducers are mounted in spanwise direction along the middle axis of the model to measure both steady and unsteady pressures. The transducers are connected with the surface of the airfoil by very short tubes. The diameter of the pressure holes on the surface is 0.7 mm. The task of the 4 accelerometers is to monitor the deformation behavior.

The wing has a rectangular planform with a chord of 0.2 m and a span of 0.1 m reaching from wall to wall. The airfoil has the theoretical coordinates of the NACA 0012 profile with maximum deviations of less than 2%. The model itself is composed of two halves; the entire leading and trailing edges are added to the upper surface of the model. In order that the model be kept reasonably lightweight, and thus have a higher natural frequency, the light metal alloy of the model shell is quite thin. The model supports are made of steel. Fiberglass-reinforced ribs inside the model provide extra rigidity. Ground vibration tests have shown that the lowest natural bending frequency for this wing configuration is over 50 Hz.

Electronic Data Recording and Processing

The portable real-time data acquisition system is designed for aeroelastic research and testing when large amounts of dynamic data are required over a wide frequency range. The scope of the present investigation included measuring the following quantities: steady pressure distributions on the model using differential pressure transducers located on the wing, unsteady pressure distributions on the model using the same differential pressure transducers, angle of attack, and oscillation amplitudes of the pitching motions by means of angle-of-rotation pickups, and the rigidity of the model by means of acceleration pickups.

The voltages of the unsteady pressures are conducted via temperature-compensated amplifiers, low-pass filters, a multiplexer, and an AD converter to the array processor. The unsteady pressures are calculated from transducer time-history data measured at a rate of $(32\times\omega/2\pi)$ samples/s (max. 400,000 samples/s). A cross-spectral analysis of the data is used to determine the magnitude and phase of the harmonic pressure coefficients or real and imaginary parts in relation to the pitch oscillation of the wing model.

The steady pressures are measured using the same differential pressure transducers as for the unsteady pressures. Ten thousand data samples were averaged for each transducer at a rate of 1000 samples/s to determine mean values of the pressure coefficients. Data were acquired simultaneously from all transducers. Aeroelastic deformation of the wing during the pressure data acquisition process can be determined by a discrete Fourier transform of time-history data measured by the accelerometers. The real-time data acquisition system is described in detail in Ref. 3.

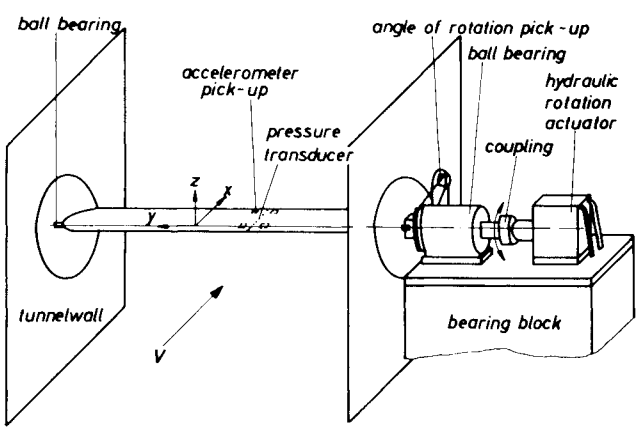

Fig. 1 Test setup.

Measuring Procedure

The pressure is measured by in situ pressure transducers. Using temperature-compensated amplifiers developed by the DFVLR in Göttingen, it is possible to measure the steady as well as unsteady pressures simultaneously with the same transducer. The advantages of this method are reduction in the costly operation time of the wind tunnel and measurement of the steady and unsteady pressures at the same location. The disadvantage of this method is the high expense of the in situ pressure transducers and the necessary electronic equipment.

The mean pressure

$$\frac{1}{T}\int_0^T p(t)\mathrm{d}t, \quad -1\ \mathrm{deg} < \Delta\alpha(t) < 1\ \mathrm{deg}$$

differs from the steady pressure (p at $\Delta\alpha \equiv 0$ deg) in the region where shock and separation occur. Figure 2 facilitates a comparison of mean and steady pressures. The differences evident in the realm where shock and separation occur are plain to see. The pressure curve of the mean pressure in the shock region is smoother.

Test Results and Discussion

It is widely known that investigations performed in wind tunnels of relatively small diameter usually require a correction of the effective angle of attack. A dependence on the resulting lift applied to the test profile cannot be ignored. The following test results of the NACA 0012 profile, however, are given without Mach number and angle-of-attack corrections. The steady pressures presented here are nondimensionalized by the dynamic pressure. In addition, the unsteady values are normalized to the amplitudes and plotted vs the nondimensional wing chord x/c. The unsteady pressure coefficients are calculated from the recorded time signals. The results are not expressed in terms of phase and amplitude, as is often the case, but in terms of real and imaginary parts, i.e., the real part is in phase with the oscillations and the imaginary part is shifted 90 deg.

Steady Results

As mentioned earlier, the steady as well as the mean pressure distributions are determined, the latter concurrently with the unsteady values. The average steady values in this case serve mainly as input into an unsteady, time-linearized, potential-theoretical transonic method,[4] which provides the first harmonic of the unsteady Δc_p distribution.

The measurements are taken without transition strip for two different Reynolds numbers. The free transition indicates a λ shock of the pressure recovery on the wing, which

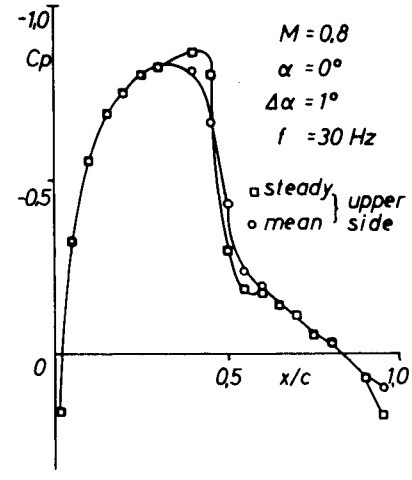

Fig. 2 Pressure patterns of the steady and mean pressure.

was confirmed by means of schlieren photography. Noteworthy differences between the results for the two Reynolds numbers occur only within the range of the greatest negative pressure, Fig. 3.

Since the parameters Mach number and angle of attack exert a great influence on the unsteady pressure distributions, the effect of these two parameters on steady pressure is analyzed as well. In Fig. 4 the nondimensional pressure c_p of the profile's upper side is presented vs the nondimensional profile chord x/c for the entire Mach number range with angle of attack $\alpha = 0$ deg. These figures show that, in the case of $M = 0.76$, the critical Mach number is exceeded although only the shock waves at $M = 0.78$ and $M = 0.8$ can be considered intense. In this case, the Reynolds number varies with the Mach number. Figure 5 shows for Mach number 0.78 the influence of the angle of attack on the steady pressure. The location of the shock wave shifts with increasing angle of attack toward the trailing edge of the profile. This process is then reversed after a certain α value has been exceeded. For angles of attack $\alpha = 5$ and 7 deg, it is clear that flow separation is caused by shock.

Unsteady Results

The scope of this paper allows only a small part of the measured unsteady pressure distribution to be presented. Results are shown that illustrate the influence of the parameters Mach number, angle of attack, reduced frequency, and oscillation amplitude. In addition, the unsteady pressures with regard to the higher harmonic parts are investigated for several particularly significant cases.

Mach Number Effects

Unsteady pressure distributions on the upper side of the model are shown in Fig. 6 for five Mach numbers in the range 0.5-0.9. The mean angle of attack is 0 deg. The oscillation amplitude is 1 deg with an oscillation frequency of 30 Hz. Accordingly, the reduced frequency ω^* ranges from 0.108-0.063 for Mach numbers $M = 0.5$-0.9.

At $M = 0.7$, the pressure curve behaves in the manner typical for subsonic flow and the critical pressure is not exceeded in this case. At $M = 0.78$ the critical pressure is markedly exceeded, forming a pressure peak that declines with the occurrence of shock. The pressure peak shifts rapidly with increasing Mach number toward the trailing edge, and the real part changes its sign at $M = 0.9$ due to the flow separation that occurs here. The sign of the imaginary part changes with the location of the shock. With regard to the phase data, the pressures ahead of the shock lag behind the motion, and those behind the shock precede the motion.

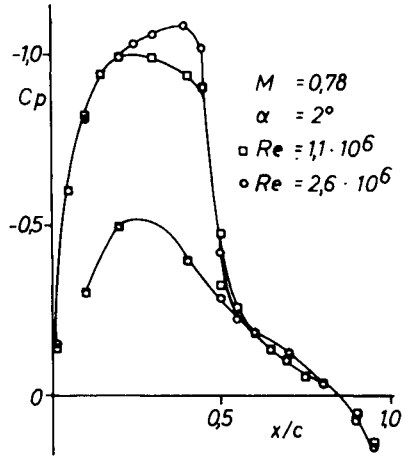

Fig. 3 Effects of Reynolds number on steady pressure.

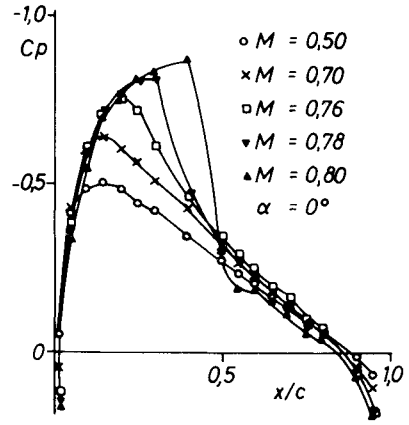

Fig. 4 Effects of Mach number on steady pressure.

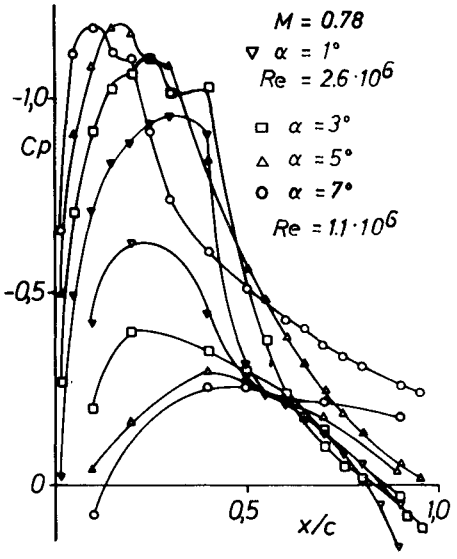

Fig. 5 Effects of angle of attack α on steady pressure.

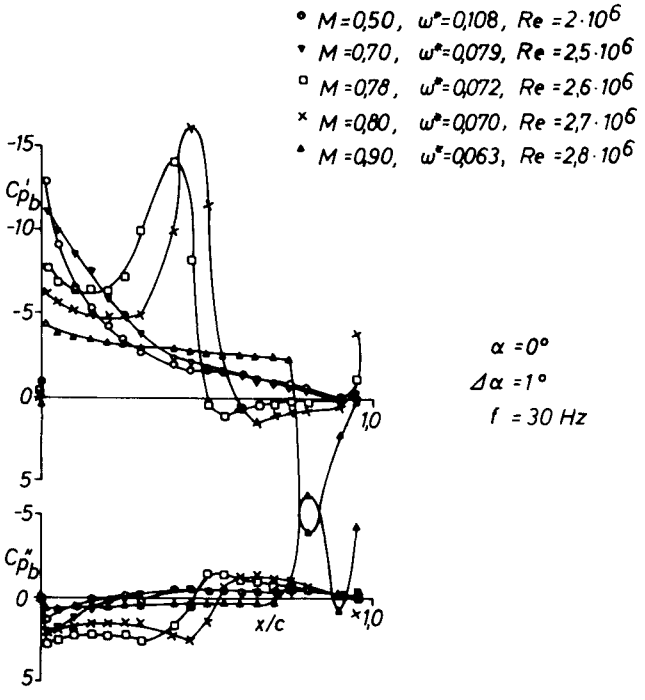

Fig. 6 Effects of Mach number on the unsteady pressure distribution on the upper side of the model.

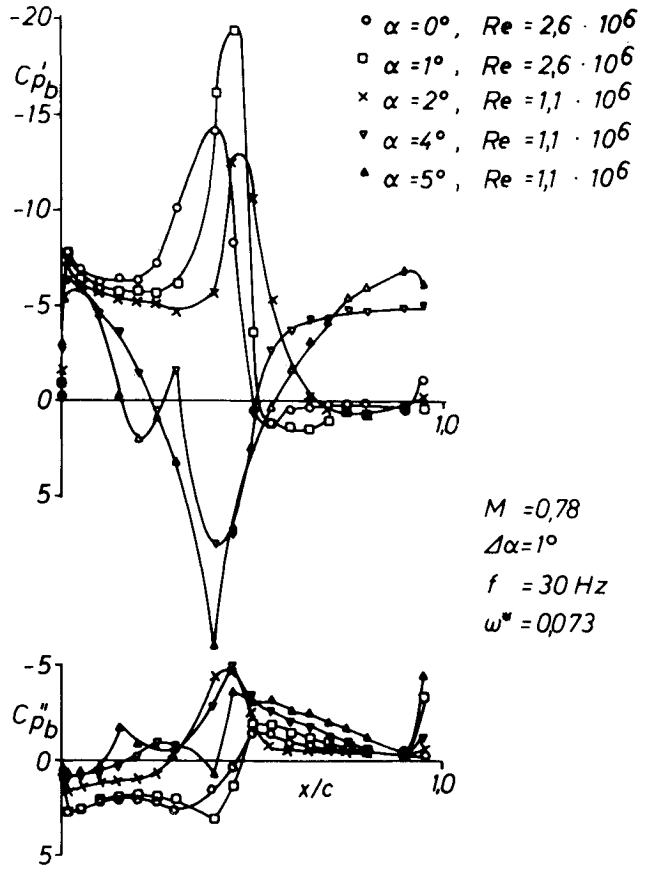

Fig. 7 Effects of mean angle of attack on the unsteady pressure distribution on the upper side of the model.

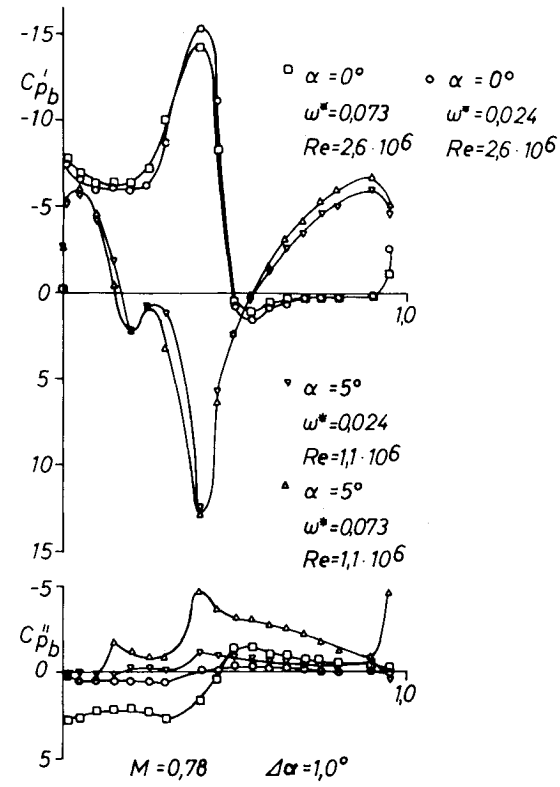

Fig. 8 Effects of oscillation frequency on the unsteady pressure distribution on the upper side of the model.

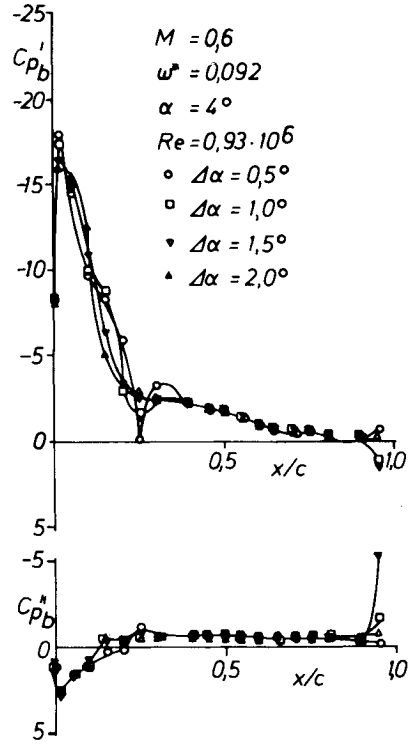

Fig. 9 Effects of oscillation amplitude on the unsteady pressure distribution; $M=0.6$, $\alpha=4$ deg.

Mean Angle-of-Attack Effects

The unsteady pressure distributions on the upper side are shown in Fig. 7 at angles of attack 0, 1, 2, 4, and 5 deg. The Mach number is $M=0.78$, with oscillation amplitude $\Delta\alpha=1$ deg, oscillation frequency $f=30$ Hz, and thus $\omega^*=0.073$. For angles of attack $\alpha=2$, 4, and 5 deg, the measurements are taken at reduced stagnation pressure, which leads to various Reynolds numbers. The shock location shifts with increasing angle of attack toward the trailing edge of the profile, until flow separation occurs at $\alpha=4$ and 5 deg, and thus the sign of the real part changes. After flow separation has occurred, the shock location appears stable as shock-induced separation at $\alpha=4$ and 5 deg continues up to the trailing edge. The influence on the mean pressure due to separation is considerably weaker than that on the unsteady pressure. The first discontinuity of the real-part pressure curve for $\alpha=4$ deg indicates that the presence of a λ shock and the magnitude of the oscillation amplitude is instrumental in determining the form of the induced λ shock. The intensity of the shock strongly influences the extent of the pressure distribution in front of the shock.

Oscillation Frequency Effects

Figure 8 shows the unsteady pressure distribution for two frequencies (10 and 30 Hz), Mach number $M=0.78$, oscillation amplitude $\Delta\alpha=1$ deg, and two angles of attack $\alpha=0$ and 5 deg. The shock location is not altered by the oscillation frequencies, and the real part of the pressure amplitude is only slightly affected. The phase, however, is shifted considerably over the imaginary part.

Oscillation Amplitude Effects

Figures 9-11 present the unsteady pressure distributions at two Mach numbers and high angles of attack for various oscillation amplitudes. Since the unsteady pressures are normalized to the oscillation amplitudes, the pressure curves are expected to coincide, assuming linear behavior. Plotted results, however, show that a slight nonlinear dependence of the unsteady pressures caused by the oscillation amplitudes occurs already in the region of low supersonic velocities, as well as in the recompression area of the flow (Fig. 9). More intense nonlinearities occur when shock waves develop due

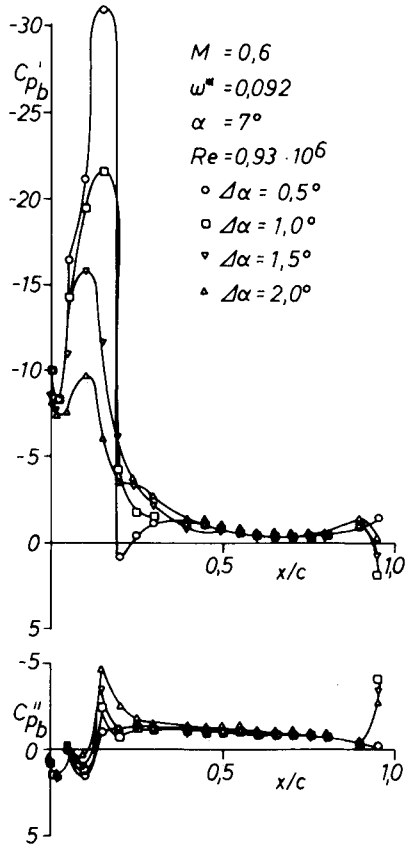

Fig. 10 Effects of oscillation amplitude on the unsteady pressure distribution; $M=0.6$, $\alpha=7$ deg.

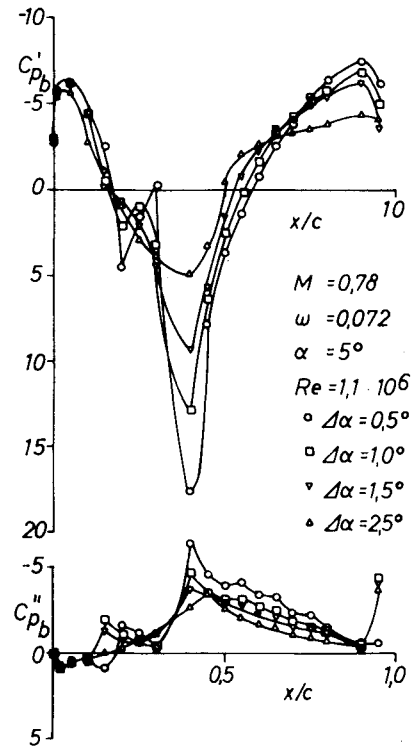

Fig. 11 Effects of oscillation amplitude on the unsteady pressure distribution; $M=0.78$, $\alpha=5$ deg.

to recompression, which completely vanish when the flow reattaches (Fig. 10). If the flow following a shock wave does not reattach, the nonlinearities do not vanish before the profile edge is reached (Fig. 11). This figure clearly shows the influence of the oscillation amplitude on the pressure curve at the site of the oblique shock of the λ shock.

Higher Harmonic Parts of Unsteady Pressure

Admittedly, a somewhat unconventional format was chosen to present the higher harmonic parts of the unsteady pressure. This was done, however, in order for the figures to accommodate as much information as possible. The amplitude values of each higher harmonic part measured are taken from the plotted power spectrum and recorded in addition to the previously determined first harmonic part (Figs. 12-14). In this process, the highest value is set at 1 and the lower values are expressed as a percentage thereof. Information on the phase term of these parts, however, is thus lost.

The unsteady pressure amplitudes appear in Fig. 12a for $M=0.6$ and $\alpha=0$ deg. In this case the critical Mach number is not exceeded and an undisturbed flow can be expected. As a result, pure harmonic excitation produces a pressure response comprising only a first harmonic part. In the case of a higher angle of attack (Fig. 12b), the critical Mach number is greatly exceeded. The resulting shock leads to a local separation of the flow, which in turn causes higher harmonic parts of the unsteady pressure. In the region of reattached flow, the higher harmonic parts vanish again. Figure 13a displays the unsteady pressure magnitude for the case of a very weak shock ($M=0.74$, $\alpha=0$ deg). Since no flow separation occurs, the higher harmonic parts are quite low, as expected. Raising the angle of attack up to just $\alpha=1$ deg causes the shock to be considerably more intense, and the separation zone is extended. As anticipated, measurement points with higher harmonic parts of the unsteady

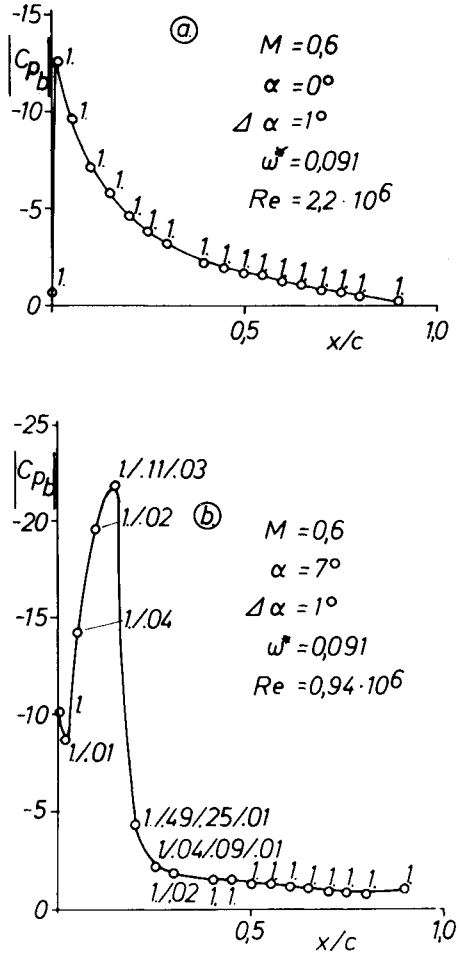

Fig. 12a, b Magnitude data of the first harmonic and of the higher harmonic unsteady pressure; $M=0.6$.

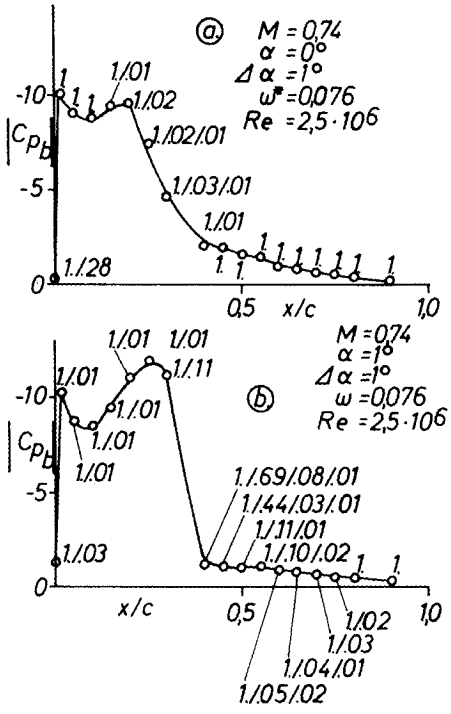

Fig. 13a, b Magnitude data of the first harmonic and of the higher harmonic unsteady pressure; $M = 0.74$.

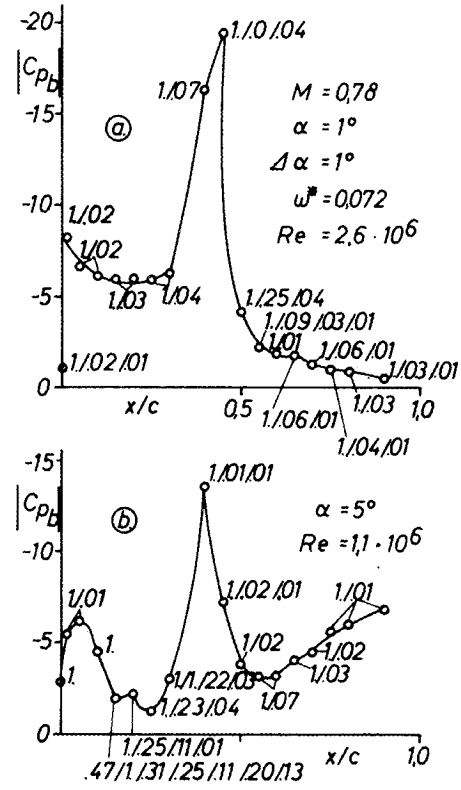

Fig. 14a, b Magnitude data of the first harmonic and of the higher harmonic unsteady pressure; $M = 0.78$.

pressure are found in this region. If the Mach number is raised to $M = 0.78$ (Fig. 14a), the shock is even more intense and the flow separation extends to the trailing edge, though greatly weakened. The oblique shock at angle of attack $\alpha = 1$ deg is not yet strong enough to cause the flow to separate. At $\alpha = 5$ deg, however, it causes a definite separation zone, which extends over the normal shock and continues up to the trailing edge (Fig. 14b). This figure shows that the higher harmonic parts constitute quite a large factor, particularly in this region of flow separation.

Comparison of Measured and Calculated Results

Calculations were performed using an unsteady time-linearized, potential-theoretical transonic method[4] in order to compare two wing configurations. For cases of small oscillation amplitudes, it is fully compatible with methods of the LTRAN[5] type but offers the advantage that mean values can be fitted or adapted to experimental investigations. In the two examples discussed here (higher subsonic and local supersonic zones with moderately intense shock), the flow is attached. Small changes of the freestream Mach number and angle of attack in the calculations lead to good agreement between steady potential theory and experimentally determined uncorrected mean values (Figs. 15 and 16). Nevertheless, the theoretical unsteady results display noticeable deviations from the corresponding experimental values (Figs. 15 and 16). Higher values for the real parts and lower values for the imaginary parts are obtained by theoretical calculation downstream from the supersonic zone (i.e., the suction tip on the upper side). The considerably higher value of the theoretically obtained imaginary part in the upstream region is the most noteworthy discrepancy here. Identical tendencies of the deviations between this theory and measurements in the same wind tunnel were observed for the supercritical MBB A3 profile.[6]

On the other hand, the agreement between previous measurements taken in the NASA Ames transonic wind tunnel[7] (likewise with pitching oscillations) is quite good.[4] This fact, coupled with the considerable differences found in the subcritical case, indicates significant wind tunnel influence, although the effects of unsteady friction are considered

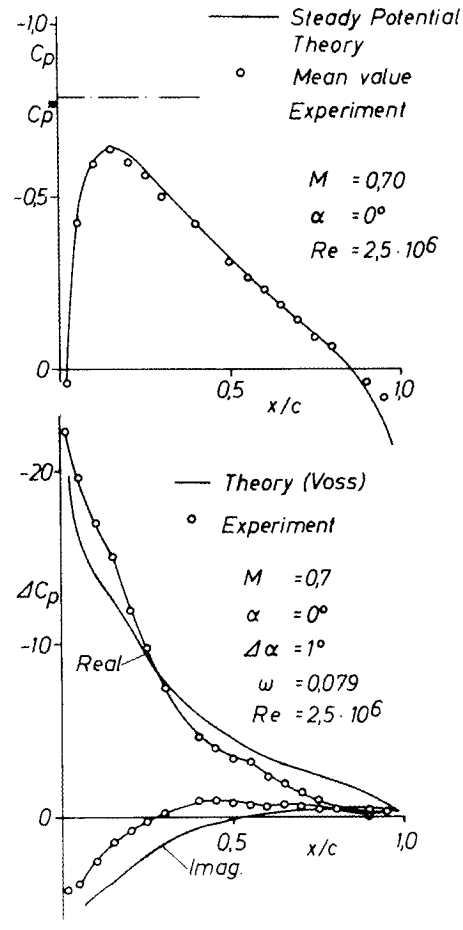

Fig. 15 Comparison between theoretical and experimental mean and unsteady pressure distributions; $M = 0.70$.

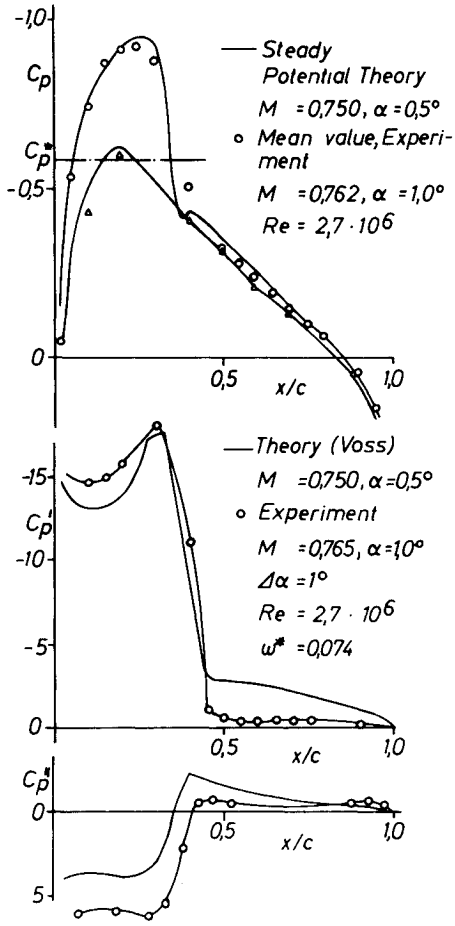

Fig. 16 Comparison between theoretical and experimental mean and unsteady pressure distributions; $M = 0.750$.

negligible. It is of course a possibility that, although the mean pressure values are identical, the field values (and thus the spatial expansion of a supersonic zone perpendicular to the profile) differ for theoretical and experimental results.

Conclusion

Steady, mean, and unsteady aerodynamic data were measured on a rectangular wing with a theoretical NACA 0012 profile in two-dimensional flow. The wing was induced to perform pitch oscillations about its c/4 axis in order to produce the unsteady data. The purpose of the tests was to provide experimental data for the development and assessment of transonic analytical codes, as well as to obtain results for flow with shock and profound separation, which are undesirable effects for passenger aircraft.

One definite result of this investigation is that both the Mach number and the angle of attack have a significant effect on the intensity and location of shock. The oscillation frequency influences mainly the phase relationship between pressure and motion, while the oscillation amplitude alters the value of the unsteady pressure, making it markedly nonlinear in the shock region at separated flow. The higher harmonic parts of the unsteady pressure occurring in this region as a result of harmonic oscillation cannot be overlooked and are dependent on the intensity of the shock.

Knowledge of the nonlinear dependence of unsteady pressure on the oscillation amplitude in addition to the occurrence of higher harmonic parts of unsteady pressure deserve particular attention with regard to the development of a practicable theoretical model for flutter calculations that does not require immediate solution of the Navier-Stokes equation. A comparison of theoretical values in the realm of nonseparated flow shows good agreement for the mean pressure values. Somewhat less satisfactory is the agreement between the unsteady pressure distributions peculiar to the region after shock, the main reason for which is most probably the influence of the wind tunnel walls.

References

[1]Carta, F. O., "Dynamic Stall of Swept and Unswept Oscillating Wings," AGARD-CPP-386, 1985.

[2]"Compendium of Unsteady Aerodynamic Measurements," AGARD Report No. 702, 1982.

[3]Weitemeier, B. and Uerlings, P., "Ein vielkanaliges Hochgeschwindigkeitsdatenerfassungssystem zur Messung und Analyse zeitabhängiger Signale," DFVLR Rept. IB 232-83 J 04, 1984.

[4]Geissler, W. and Voss, R., "Investigation of the Unsteady Airloads on Airfoils with Oscillating Control in Sub- and Transonic Flows," *Proceedings of the International Symposium on Aeroelasticity,* DGLR Rept. 82-01, 1982, pp. 65-80.

[5]Ballhaus, W. F. and Goorjian, P. M., "Implicit Finite-Difference Computations of Unsteady Transonic Flows about Airfoils," *AIAA Journal,* Vol. 15, Dec. 1977, pp. 1728-1735.

[6]Triebstein, H. and Voss, R., "Transonic Pressure Distributions on a Two-Dimensional 0012 and Supercritical MBB-A3 Profile Oscillating in Heave and Pitch," AGARD-CP-374, 1985.

[7]Davis, S. S. and Malcolm, G. N., "Experimental Unsteady Aerodynamics of Conventional and Supercritical Airfoils," NASA TM 81221, Aug. 1980.